The VLF transmitters' radio wave anomalies related to 2010 Ms 7.1 Yushu earthquake observed by DEMETER satellite and the possible mechanism

Shufan Zhao[1][*], XuHui Shen[1], Zeren Zhima[1] and Chen Zhou[2]

[1] Institute of Crustal Dynamics, China Earthquake Administration, Beijing 100085, China

[2] School of Electronic Information, Wuhan University, Wuhan, 430072, China

* Correspondence: zsf2008bj@126.com

Abstract: Earthquakes may disturb the lower ionosphere through various coupling mechanisms during the seismogenic and coseismic periods. The VLF signal radiated from ground-based transmitters will be affected when it penetrates the disturbed ionosphere above the epicenter area, and this anomaly can be recorded by low earth orbit satellite under certain conditions. In this paper, the temporal and spatial variation of the Signal to Noise Ratio (SNR) of the VLF transmitter signal in the ionosphere over the epicenter of 2010 Yushu Ms 7.1 earthquake in China is analyzed using DEMETER satellite observation. The results show that the SNR over the epicenter of Yushu earthquake especially in the southwestern region decreased (or dropped) before the main shock, and GPS-TEC anomaly accompanied which imply that the decrease of SNR might be caused by the enhancement of TEC. A full-wave method is used to study the mechanism of the change of SNR before the earthquake. The simulated results show SNR does not always decrease before an earthquake. When the electron density in the lower ionosphere increases by three times, the electric field will decrease about 2 dB, indicating that the disturbed electric field decrease 20% compared with the original electric field and vice versa. It can be concluded that the variation of electron density before earthquakes may be one of the important factors influence the variation of SNR.

Keywords: 2010 Yushu earthquake, DEMETER satellite, VLF radio wave, signal to noise ratio, lower ionospheric disturbance, Full-wave model

1. Introduction

The VLF (Very Low Frequency) radio waves radiated by the powerful ground-based VLF transmitters have been used for long distance communication and submarine navigation, because of the efficient reflection within the earth-ionosphere waveguide. However, there is still a small fraction of the wave energy that can leak into the higher ionosphere and magnetosphere after being absorbed intensively by the lower ionosphere. The signals from transmitters observed by the LEO (Low Earth Orbit) satellite can be used to study the propagation of VLF wave in the earth-ionosphere waveguide and ionosphere, as well as wave-particle interaction in the radiation belt (Inan et al., 2007; Inan and Helliwell, 1982; Lehtinen and Inan, 2009; Parrot et al., 2007).

It is gradually confirmed that earthquake precursors not only appear near the ground, but also may couple with the atmosphere and ionosphere through some mechanisms, resulting in plasma disturbances in the ionosphere and recorded by various instruments like ionosonde or GPS receivers measuring TEC (Total Electron Content) (Liu et al., 2009; Liu et al., 2001; Liu et al., 2006; Pulinets et al., 2000; Stangl et al., 2011;

Zhao et al., 2008). Therefore, the amplitude of the VLF signals from the ground-based VLF transmitter observed on the ground and satellite from will change when encounter the disturbed area in the ionosphere (Hayakawa, 2007; Maurya et al., 2016; Molchanov et al., 2006; Píša et al., 2013). Molchanov et al. (2006) have found the SNR (Signal to Noise Ratio) of the electric field from VLF transmitters recorded by DEMETER (Detection of Electro-Magnetic Emission Transmitted from Earthquake Regions) satellite decreased near the epicenters during a series of earthquakes. The spatial size of SNR reduction zone increases with the magnitude of the earthquake. However, it is hard to distinguish the coseismic anomaly and precursor from their results.

Two devastating earthquakes, the 2008 Ms 8.0 Wenchuan earthquake and the 2010 Ms 7.1 Yushu earthquake, have occurred successively in southwestern China during the operation period (2004-2010) of DEMETER satellite. Some research have also focused on the SNR variation of VLF transmitters using DEMETER satellite observation to extract the earthquake related anomalies before the two strong earthquakes (He et al., 2009; Shen et al., 2017; Yao et al., 2013). The results all illustrated the decrease of SNR before the earthquakes. Since the earthquake related-ionospheric disturbance zone is not right over the epicenter, the relative position of the SNR anomaly and the epicenter should be furtherly studied. The factors which influence the SNR and the possible mechanism is also needed to be comprehensively illustrated.

The Alpha VLF transmitters in Russia transmit three frequencies in each station which provide us opportunities to study the influence of the ionosphere on different wave frequencies. The devastating earthquake nearest the transmitters in China is 2010 Ms 7.1 Yushu earthquake. In this paper we investigate the temporal and spatial SNR variation of the VLF transmitter signal in the ionosphere near the epicenter of the Yushu earthquake using DEMETER observation. The background variations of SNR in the same period of 2007-2010 have also been studied to distinguish whether the SNR reduction is caused by earthquake or just ionospheric background changes. The mechanism of how the seismo-ionospheric disturbance affect the variation of SNR has been discussed in this paper.

As the mechanism of the VLF radio wave variations in the altitude of LEO satellite (presented as SNR variation) before the earthquakes, Hayakawa (2007) and Píša et al. (2013) suggest the VLF anomalies exist because the lower ionosphere is lowered before earthquake. Molchanov et al. (2006) declared that the variation of SNR of satellite data is attributed to the ionospheric disturbance, especially the lower ionospheric disturbance. Furthermore, it has been found that the electron density variation could exists in the lower ionosphere according to the computer ionosphere tomography (CIT) results based on GPS-TEC data before Nepal Ms 8.1 earthquake in 2015 (Kong et al., 2018). The electric field penetrating model of shown that the electron density and height of the lower ionosphere can be changed by the additional current in the global electric circuit before the earthquake. On the other hand, Marshall et al. (2010) construct a 3D finite difference time domain model to simulate the lightning could also cause the disturbance of the electron density in the lower ionosphere which has similar mechanism as the earthquake. Many studies also have found the main loss of VLF wave power mainly occurs in the D/E region of the ionosphere when the wave penetrates into ionosphere (Cohen and Inan, 2012; Liao et al., 2017; Starks et al., 2008; Tao et al., 2010; Zhao et al., 2017; Zhao et al., 2015). In sum, the electron density variation in the lower ionosphere might be one main factor causing the SNR anomaly of VLF transmitter signal in the ionosphere. Based on these results, the full-wave calculation model was utilized to study the influence of the electron density disturbance of the lower ionosphere on the variation of VLF radio signals.

In this paper, a brief description of the DEMETER data and full-wave method used in this study are presented in Section 2. The temporal and spatial variations of SNR over the epicenter have been investigated before the Yushu earthquake with four years (2007-2010) data; the full-wave model is used to simulate how the variation of electron density in the lower ionosphere affects the SNR of the electric field from VLF transmitter at the altitude of satellite in Section 3. The discussion and conclusions of this study are presented in Section 4 and 5 separately.

2. Materials and Methods

2.1. Earthquake, VLF Transmitters, and DEMETER data

At the local time 07:49:37.9 of April 14, 2010, a Ms 7.1 earthquake hit the Yushu city, Qinghai Province with epicenter is in 33.2° N, 96.6° E with a 14 km depth at the Northeastern Tibetan plateau. The nearest VLF transmitter around the epicenter is in the proximity of Novosibirsk (NOV, in short) which belongs to the Russian Alpha navigation system which consists of three transmitters. The other two transmitters named Krasnodar (KRA) and Khabarovsk (KHA) are far away from Yushu earthquake, so only the satellite data radiated from NOV have been used to analyze in this paper. The location of the transmitters and the epicenter of Yushu earthquake are denoted by blue squares and black stars respectively in Figure 1. Each transmitter radiates three different frequency VLF radio signals (11.9/12.6/14.9 kHz), with a 0.4 s duration and a 3.6 s cycle.

The DEMETER satellite was launched on 29 June 2004 as a sun-synchronous orbit at the altitude of 710 km, then was changed to 660 km in December 2005 (Parrot et al., 2006), and the operation was ended in December 2010. The scientific objective of the DEMETER is to detect and characterize the electromagnetic signals associated with natural phenomena (such as earthquakes, volcanic eruptions, tsunamis) or anthropogenic activities. It operated in the region from invariant latitude -65° to 65°, with descending and ascending orbits crossing the equator at local time ~10:00 and ~22:00, respectively. DEMETER has a re-visit orbit period of about 14-days, which means the satellite returns over the same orbit trajectory after 13 days. The payloads include several electromagnetic sensors with two working mode: burst and survey. At ELF/VLF band, the intensive electromagnetic wave data over locations of particular interest were provided in the burst mode, and in the survey mode, electric and magnetic power spectral density (PSD) data every 2 s were provided with sampling frequency 40 kHz and spectral resolution 19.53 Hz.

According to the formula of Dobrovolsky et al. (1979),the preparation zone of the earthquake can reach $\rho=10^{0.43M}$, where M is the magnitude of the earthquake and ρ is measured in km. Considering the limited extension of the Ms 7.1 Yushu earthquake, the preparation zone ρ can reach to 1130 km, we mainly focused on the region within the region of epicenter ±10° (black square in Figure 1). In this study, the night-time PSD data of electric field from the DEMETER's survey mode observations were extracted study the perturbations of the VLF signal before and after the Yushu earthquake. Due to the VLF radio signals at daytime is too small and to cause obvious SNR variation compared with that in night-time, we did not use the day-time data in this study.

2.2. The method to calculate SNR

According to the method of Molchanov et al. (2006), the SNR of electric field was calculated as follows:

114
$$SNR = \frac{2A(f_0)}{A(f_+)+A(f_-)} \quad (1)$$

115 where A(f₀) is the amplitude of electric field spectrum at the central frequency, and $A(f_\pm)$ are the

116 spectrums at $f_\pm = f_0 \pm \Delta f$, where Δf is the chosen frequency band. For the three Russian VLF

117 transmitters, the f_0 is set as three VLF radio waves frequency radiated from NOV transmitters:

118 11.9/12.6/14.9 kHz, and the Δf=300 Hz.

119 *2.3. Full wave method*

120 A full-wave method has been used to seek a solution of Maxwell equations for waves varying as $e^{j\omega t}$ in

121 a horizontally-stratified medium with fixed dielectric permittivity tensors $\hat{\varepsilon}$ and permeability μ in each layer.

122 Considering the region of our interest is much smaller than the radius of the earth, the earth's curvature is

123 neglected in this study. A Cartesian coordinate system is established with x, y in the horizontal plane and z

124 vertical upward. We seek a solution of the Maxwell equations in a form of a linear combination of plane waves

125 $\sim e^{j(k_\perp \cdot r_\perp)}$, where $k_\perp$ is the horizontal component of the wave vector k which is conserved by Snell's law

126 inside each layer, we have

127
$$\begin{cases} k \times E = \omega\mu_0 H \\ k \times H = -\omega\hat{\varepsilon}E \end{cases} \quad (2)$$

128 Where ω is the angular frequency, μ is the permeability of the medium ($\mu \equiv 1$ for non-magnetic

129 medium), $\hat{\varepsilon} = \varepsilon_0(I + \hat{\chi})$ is dielectric tensor, and $\hat{\chi}$ is electric susceptibility tensor (Yeh and Liu, 1972). $\hat{\chi}$ is

130 determined by the electron density and collision frequency in the ionosphere, as well as the geomagnetic field.

131 In our simulation, the electron density is calculated by International Reference Ionosphere (IRI) model (Bilitza

132 et al., 2017), and the electron collision frequency (denoted by v) is modeled by the exponential decay law

133 with the height (denoted by *h*) increasing $v=1.8\times10^{11}e^{-0.15h}$. The parameters of geomagnetic field at the

134 location of VLF transmitter is calculated by International Geomagnetic Reference Field (IGRF) model (Finlay

135 et al., 2010).

136 Eliminating the z components from equation (2), we can obtain the following elegant form of Maxwell

137 equations:

138
$$\frac{dV}{dz} = jk_0\hat{T} \cdot V \quad (3)$$

139 Where $V = (E_\perp, Z_0H_\perp)$, Z_0 is wave impedance, $\hat{T}$ is a 4×4 matrix:

140
$$\widehat{T} = \begin{pmatrix} -\frac{k_x\varepsilon_{31}}{k_0\varepsilon_{33}} & -\frac{k_x\varepsilon_{32}}{k_0\varepsilon_{33}} & \frac{k_xk_y}{k_0^2\varepsilon_{33}} & 1-\frac{k_x^2}{k_0^2\varepsilon_{33}} \\ -\frac{k_y\varepsilon_{31}}{k_0\varepsilon_{33}} & -\frac{k_y\varepsilon_{32}}{k_0\varepsilon_{33}} & -1+\frac{k_y^2}{k_0^2\varepsilon_{33}} & -\frac{k_xk_y}{k_0^2\varepsilon_{33}} \\ -\varepsilon_{21}+\frac{\varepsilon_{23}\varepsilon_{31}}{\varepsilon_{33}}-\frac{k_xk_y}{k_0^2} & -\varepsilon_{22}+\frac{\varepsilon_{23}\varepsilon_{32}}{\varepsilon_{33}}+\frac{k_x^2}{k_0^2} & -\frac{k_y\varepsilon_{23}}{k_0\varepsilon_{33}} & \frac{k_x\varepsilon_{23}}{k_0\varepsilon_{33}} \\ \varepsilon_{11}-\frac{\varepsilon_{13}\varepsilon_{31}}{\varepsilon_{33}}-\frac{k_y^2}{k_0^2} & \varepsilon_{12}-\frac{\varepsilon_{13}\varepsilon_{32}}{\varepsilon_{33}}+\frac{k_xk_y}{k_0^2} & \frac{k_y\varepsilon_{13}}{k_0\varepsilon_{33}} & -\frac{k_x\varepsilon_{13}}{k_0\varepsilon_{33}} \end{pmatrix} \tag{4}$$

141 The electromagnetic field in each layer can be obtained in the k (wave vector) domain by solving equation (3)

142 recursively in a direction which provides stability against the numerical "swamping" (Budden, 1985; Lehtinen

143 and Inan, 2008). The difficulty is how to deal with numerical stability when the solution of evanescent wave

144 "swamp" the waves of interest because of the large imaginary of the vertical wave number. More details of full-

145 wave method is described in Lehtinen and Inan (2008).

146 **3. Results**

147 *3.1. VLF signal analysis from DEMETER satellite*

148 The SNR 5 re-visit periods before and 1 re-visit period after the earthquake in 2010 were calculated to

149 study the evolution of SNR above the epicenter. The SNR distributions of three frequencies (11.9, 12.6, 14.9

150 kHz) within the region of epicenter ±10° are shown in Figure 2, where the value of SNR is denoted with colored

151 dots with different size and the black star represents the epicenter of Yushu earthquake. The data when has

152 geomagnetic storms (here we defined Kp>3 and Dst< -30 nT) was plotted with hollow dots, and grey dots is

153 very small means the transmitter is turned off on these days. It can be found that in the 1st re-visit period (April

154 2-14) before the earthquake, the SNR of three frequencies all decrease dramatically compared with other periods

155 no matter before or after the earthquake. In the first re-visit period from April 2 to 14 in 2010, there are two

156 magnetic storms occurred on April 4-7 and April 11-12, respectively.

157 To minimize the impact of other factors and confirm whether the SNR anomaly is caused by earthquake

158 not the variation of the ionospheric background, we focus on the SNR in the black square (shown in Figure 1)

159 of the same period in 2007-2009 as background when there are no large earthquakes and the data when the

160 transmitter was turn off or affected by geomagnetic storms are eliminated. The mean value of all the data in

161 each period has been obtained to get the time sequence shown in Figure 3. In Figure 3, the black dashed line

162 represents the occurred date of the earthquake. The black and red solid lines represent the average values in 5

163 periods before the earthquake and 1 period after the earthquake within the region of epicenter ±10° in 2010 and

164 background time, respectively. The change trends of SNR in background time and 2010 are the same except in

165 the 1st period before the earthquake. In the 1st period before the earthquake the SNR decreased significantly in

166 2010 while it increased in background time at all transmitting frequency. It means the decrease of SNR in the

167 1st period in 2010 might be caused by Yushu earthquake.

168 The above results use the average value within the region of epicenter ±10° in one revisit period of

169 DEMETER to analyze the anomalies which ignore the day-to-day variability of the ionosphere. Furtherly, the

170 daily variation of SNR in the 1st period before the earthquake is studied using a quartile-based process (Liu et

171 al., 2009) to detect the anomaly of the SNR. The median (M), the lower (first) quartile (denoted as LQ in short)

172 and the upper (third) quartile (UQ in short) of every successive 11 days of the SNR of the orbits data within the

173 region of epicenter ±10° has been calculated to find the deviation between the observed SNR of the 12th day

174 and the computed median (M). Based on the assumption of the normal distribution of the SNR with the mean

175 (m) and standard deviation (σ), the expected value of M and LQ or UQ are equals to m and 1.34σ ((Liu et al.,

176 2009) and reference therein). We set the lower boundary (LB in short), LB = M+2(M-LQ) and the upper

177 boundary (UB in short), UB= M+2(UQ-M) to find the SNR anomalies with a stricter criterion. Thus, if an

178 observed SNR on the 12th day is greater or smaller than its previous 11-day-based UB or LB, a positive or

179 negative anomaly of SNR will be identified. Figure 4 shows the time series of SNR at 11.9, 12.6, 14.9 kHz, and

180 the red, gray, black curves denote the current SNR, associated median and upper/lower boundary (UB/LB),

181 respectively. Blue and green markers represent the positive and negative anomaly. As shown in Figure 4,

182 besides the negative anomalies appeared on April 13 (one day before Yushu earthquake, the occurred time of

183 Yushu earthquake denoted by vertical dashed line in Figure 4) at all transmitting frequency, there are another

184 three anomalies occurred on March 29, April 8,and April 10 respectively. Previous researches indicate the

185 earthquake anomaly usually occurred within one week before earthquake, so the negative anomaly occurred on

186 March 29 at 12.6 and 14.9 kHz may be not related with Yushu earthquake. The anomalies on April 8 and April

187 10 only occurred on one single transmitting frequency, which maybe do not have significance and is needed to

188 be further researched.

189 The result in Figure 4 shows the anomalies of SNR during successive 20 days before Yushu earthquake.

190 However, the 20-day orbital data may be carried into the ionospheric background noise of different space. To

191 avoid this kind of ionospheric background noise, we select the three revisit orbits to analyze the anomalies of

192 SNR before Yushu earthquake furtherly (the revisit orbit on April 9 overhead the epicenter, the revisit orbit on

193 April 13 which is 550 km away from epicenter, the revisit orbit on April 10 which is 750 km away from

194 epicenter are selected). The quartile-based process is also performed on every revisit orbital data, but 6 days'

195 sliding mean value (including 3 days before current day, 2 days after current day) have been analyzed. The

196 green and blue bar represents negative and positive anomalies in one orbit respectively in Figure 5. As we can

197 see in the top and middle panel, in the April 9, 10, the negative and positive anomalies both occurred like other

198 days in the same two revisit orbits. These anomalies could be induced by the daily variation. In the bottom

199 panel, there are no obvious anomalies in other days with the same revisit orbit of April 13, but the SNR have

200 obvious negative anomalies on all the orbit of April 13. These results further confirm that the anomalies of SNR

201 occurred on April 13.

202 We speculate that the anomalies of SNR may be related to the anomalies of electron density. To confirm

203 our conjecture, we used GPS-TEC MAP data distributed by CODE (Center for Orbit Determination in Europe)

204 to check out whether the Total electron content (TEC) showing similar anomalies. The resolution of TEC data

205 from CODE is 5°×2.5°, We use 11 days' sliding mean value of every grid as background, then we can get a

206 spatial distribution of background. Background ± 2×stand deviation is set as threshold (Upper bound and Lower

207 bound) to determine whether there have anomalies, if intraday value exceed the threshold represents there have

208 anomalies. We have reviewed the TEC anomalies of every day from April 2 to April 14 (which means the

209 duration of sliding background is from March 22 to April 13). The TEC anomalies only occurred April 13,

210 especially the anomalies are the most intensive at UT 6:00 which means only the SNR anomaly at April 13 is

211 possible earthquake precursory, the other two anomalies at April 8 and 10 in Figure 4 may be caused by other

212 factors. The top panel of Figure 6 shows the TEC at 6:00 am UT on April 13 and the sliding mean of background

213 (April 2-12), the bottom panel shows the abnormal region where the TEC value exceed threshold (background
214 ± 2×stand deviation). As we can see that the TEC had abnormal enhancement on April 13 at southwestern
215 region of epicenter. In addition, we collect the COSMIC data in the abnormal region of TEC (southwestern
216 region of Yushu epicenter) to check whether there is abnormal variation in D/E region electron density. As
217 shown in Figure 7, the result shows it indeed exist disturbance in E region on April 13. Similar to the abnormal
218 region of electron density, the SNR of orbit No. 030939-1 on April 13 also decreased in the southwestern
219 direction in Figure 2. This phenomenon maybe illustrates the decrease of SNR caused by TEC enhancement.
220 Furthermore, this TEC enhancement was probably caused by earthquake, because it shows very intensive
221 conjugate response. However, TEC anomalies caused by geomagnetic storm do not exhibit this kind of
222 phenomenon generally(Zhao et al., 2008).

223 *3.2. The possible mechanism of SNR variation revealed by full-wave simulation*

224 In section 3.1, we analyzed the spatial and temporal characteristics of SNR during the five-revisit period
225 before and one revisit period after the Yushu earthquake. It can be found that the SNR decreased significantly
226 before the earthquake over the epicenter area of Yushu earthquake, especially in the southwestern direction.
227 After excluding the influence of geomagnetic storms, we furtherly explored the possible mechanism of SNR
228 abnormal variation in this section. As mentioned in the section 1, the electron density in the lower ionosphere
229 can be disturbed through various mechanisms before earthquakes. The electron density before Nepal earthquake
230 was obtained from computer ionosphere tomography method by using GPS data (Kong et al., 2018).Their
231 results shows the abnormal variation of electron density occurred at the height of 150 km before Nepal
232 earthquake and the range of variation reaches about 30%. However the electron density hardly change at the
233 height of 450 km. Marshall et al. (2010) have shown that 60 horizontal discharge pulses of 7 V/m near the
234 ground can cause 50% change of electron density in lower ionosphere, and 60 horizontal discharge pulses of 10
235 V/m near the ground can even cause 400% change of electron density. The variation of electron density in the
236 ionosphere caused by lightning activity and earthquake can both be explained by one Lithosphere-Atmosphere-
237 Ionosphere Coupling mechanism, penetration of DC electric field (Zhou et al., 2017; Kuo et al., 2011). These
238 results provide us a reference on the amplitude of the perturbation of the electron density in the D/E region.
239 Based on these results, the full-wave model was used to simulate the changes of the electric field at satellite
240 altitude excited by ground-based VLF transmitter caused by the enhancement or decrease of electron density in
241 the lower ionosphere, so as to furtherly determine the change law of SNR.

242 As mentioned in the introduction, the major VLF wave energy almost lost in the D/E region, after that, the
243 radio wave penetrate to topside ionosphere even magnetosphere with a minor linear reduction because the mode
244 conversion (Lehtinen and Inan, 2009; Shao et al., 2012). The data of COSMIC also illustrate the anomaly of
245 electron density not only occurred in the F region (represented by anomaly of TEC), but also occurred in the
246 D/E region, so the full wave method (FWM) (Lehtinen and Inan, 2009) was utilized to simulate the electric
247 field between altitudes of 0 - 120 km induced by NOV transmitter which is the closest transmitter to epicenter
248 of Yushu earthquake. Considering that the study area is much smaller than the radius of the Earth, the Earth's
249 curvature was neglected in this study. A Cartesian coordinate system was established with x, y in the horizontal
250 plane and z vertical upward.

251 We set a Gaussian shape perturbation at 110 km with 20 km standard deviation in the ionosphere. The
252 magnitude of the perturbation was set as maximum 1.3 and 4 times both increase and decrease compared to the

original electron density of nighttime (the average electron density above NOV transmitter during 20100402-20100414 at LT 22:00 calculated from IRI-2016 model). The perturbation patterns are shown in the Figure 8 using 4 times increase and decrease compared to the original electron density as example. The electron collision frequency is modeled by the exponential decay law described in the section 2.3. The geomagnetic field intensity and inclination at the location of the NOV transmitter are calculated by IGRF model.

The electric field only from ground surface to 120km have been calculated by full wave model, Because the electromagnetic wave at VLF band will propagate upward as whistler mode. The group velocities of the upward radiated whistler-mode are almost parallel, and these waves form a narrow-collimated beam which does not have much lateral spread. The direction of group velocities is determined by refractive index surface. The refractive index surface of the upgoing whistler mode at 120km is shown in Figure 9. A ducted propagation is adopted at this L shell (Clilverd et al., 2008) and the VLF wave power is spread in accordance with the divergence of geomagnetic field lines with a linear reduction because the mode conversion (Lehtinen and Inan, 2009; Shao et al., 2012). The abnormal region of TEC and SNR both occurred in the southwestern region of Yushu epicenter could demonstrated the VLF radio wave propagate in ducted mode.

The simulated results of electric field at 120 km height with different electron density along the magnetic meridian plane within 1000 km area around the transmitter NOV with 11.9 kHz transmitting frequency are shown in Figure 10. The simulated results are similar when the transmitting frequency is 12.6 kHz and 14.9 kHz. It can be seen that the wave mode interference in the wave-guide has been mapped into the ionosphere in the electric field (Lehtinen and Inan, 2009), and the electric field increases when the electron density decreases, and vice versa (Figure 10a,c). Furthermore, the maximum value of the electric field varying with height is collected to study the influence of the electron disturbance. In the nighttime, when i the variation of electron density is smaller, the variation of electric field is also smaller (Figure 10b,d). When the electron density increases by four times, the maximum electric field decreases about 2 dB at 120 km (see Figure 10d). The variation is also 2 dB at DEMETER's altitude (660 km) because of the linear reductions (Lehtinen and Inan, 2009; Shao et al., 2012), which implies that the disturbed electric field decrease 20% compared with the original electric field (Figure 8b). In a short time-interval as a few days before the earthquake, the background noise can be assumed stable, so the change of electric field can reflect the change of SNR. It can be concluded when the electron density increases by four times, the variation of SNR is 20%. The simulated results illustrate that the variation of electron density in the lower ionosphere before earthquake is one main factor of causing the abnormal variation of SNR. The more precise SNR variation needs more observation and simulation in the future.

4. Discussion

4.1. The possible mechanism on how the earthquake induces the disturbance in the lower ionosphere

Which coupling mechanism is effective to induce electron density anomalies in the D/E layer by earthquakes is still an open question. Molchanov et al. (2006) declared the lower ionospheric disturbance is caused by acoustic gravity wave triggered by earthquakes. At present, the coupling mechanism of electric field proposed by Pulinets (2009) is widely accepted because it has been demonstrated by a series models (Kuo et al., 2011; Namgaladze et al., 2013; Zhou et al., 2017) and observations (Gousheva et al., 2006; Gousheva et al., 2008; Li et al., 2017). As for 2008 Wenchuan Ms 8.0 earthquake in China, Li et al. (2017) reported continuous

292 observations about the anomalous electric field which lasted longer but weaker than the electric field induced

293 by lightning during one month before Wenchuan earthquake, which suggests that the abnormal electric field

294 might be caused by the seismogenic activity of Wenchuan earthquake. Xu et al. (2011) also found about 2

295 mV/m anomalous electric field in the F2 layer of ionosphere before the Wenchuan earthquake. Gousheva et al.

296 (Gousheva et al., 2006; Gousheva et al., 2008) revealed a large number of anomalous electric fields before

297 earthquakes using the Intercosmos satellite. In addition, it is demonstrated that the anomalous electric field

298 induced by earthquake could change the electron density in the lower ionosphere by Kuo et al. (2011) and Zhou

299 et al. (2017). Such as 2015 M 8.1Nepal earthquake, the electron density variation was well explained by the

300 ground electric field coupling model established by Zhou et al. (2017).

301 *4.2. The other factors may induce disturbance in the lower ionosphere*

302 The lightning, geomagnetic storms and other natural sources may induce disturbance in the lower

303 ionosphere (Marshall et al., 2010; Maurya et al., 2016; Peter et al., 2006; Zigman et al., 2007). As known, the

304 intensive TEC change occurs during geomagnetic storms, and the change of TEC is affected intensively during

305 the main phase of the geomagnetic storm, gradually return to normal accompany with the recovery phase. To

306 avoid the effect of geomagnetic storms, the data which kp > 3 and Dst < -30 nT were excluded in this research

307 and the TEC anomaly detected in Figure 6 showed on one day after the recovery phase of geomagnetic storm

308 (top panel of Figure 11). Furthermore, the change pattern of TEC is totally different from the one caused by

309 earthquake, because the TEC anomalies caused by geomagnetic storm expand from high-latitudes to mid-

310 latitudes due to thermospheric neutral winds, E×B convection and so on (Pokhotelov et al., 2008). From bottom

311 panel of Figure 11, we can see the SNRs on the whole orbit are large in April 5,6,7 and 11 during geomagnetic

312 storm, especially at the higher latitude. However, SNR pattern in April 13 is totally different, the SNRs on the

313 orbit of April 13 only decrease at the abnormal TEC region. In sum, The TEC anomaly on April 13 should be

314 unconcerned with geomagnetic storm. The lightning flash is very rare in our research region (only 4 events

315 from Feb 2010 to Apr 2010, which can be get from the search result of website

316 (https://lightning.nsstc.nasa.gov/nlisib/nlissearch.pl?coords=?579,18)), so the effect of lightning could be

317 ignored in this study.

318 **5. Conclusions**

319 In this paper, the SNR of electric field from ground based VLF transmitter observed by DEMETER

320 satellite was analyzed before and after 2010 Ms 7.1 Yushu earthquake. The VLF signals from Russian VLF

321 transmitters can be clearly observed at frequency of 11.9, 12.6, 14.9 kHz over the epicenter from the electric

322 field spectrum data. To determine whether the SNR variation is related to Yushu earthquake, the data in quiet

323 space weather conditions (kp ≤3 and Dst ≥ -30 nT) have been selected during five satellite revisit periods before

324 the earthquake and one revisit period after the earthquake. The result shows that the SNR decreased during one

325 revisit period before Yushu earthquake in all case. Our analysis on SNR variation also shows that the SNR in

326 April 13 is smaller than that in other days over the epicenter, the day to day variation of revisit orbit also

327 demonstrate this point, and the decrease of SNR is the most intensive at the southwestern region when we divide

328 the space over the epicenter of earthquake into four regions. These results are consistent with the TEC anomalies

329 in Figure 6. In addition, we also analyzed the SNR changes over the epicenter in the same period from 2007-

330 2010 as background map and found that the SNR changes trend of one revisit period before the earthquake

relative to background time were contrary to those in 2010. The change trend of SNR decreased in 2010 but increased in background time in the 1st revisit period before the earthquake. The change trend of SNR is the same in other revisit period both in 2010 and background time. In sum, it can be concluded that the SNR over the epicenter of Yushu earthquake decreases abnormally in one satellite revisit period before the earthquake, especially in the southwestern region of the earthquake, which is consistent with the observed TEC anomaly before the earthquake. The decrease of SNR before the Yushu earthquake may be due to the enhancement of electron density.

The electron density in the lower ionosphere may change abnormally before earthquake through some coupling mechanisms. The full wave simulation result on NOV transmitter, which is the nearest transmitter next to Yushu earthquake, indicates that the electric field at the altitude of satellite will change when we add a disturbance on electron density in the lower ionosphere. That is to say that the SNR of electric field will also change when the background noise is considered to be invariable a few days before the earthquake. The simulated results show SNR does not always decrease before an earthquake like some previous reports show(He et al., 2009; Molchanov et al., 2006; Yao et al., 2013), which depends on the change of electron density. The SNR of electric field will decrease with the increase of electron density in the lower ionosphere; the SNR will increase with the decrease of electron density in the lower ionosphere. It can be concluded that the variation of electron density before earthquakes may be one important factor influence the variation of SNR.

We will continually explore the law of SNR change and verify the mechanism we proposed with more seismic events, by utilizing the newly launched LEO electromagnetic satellite (China Seismo-Electromagnetic Satellite) (Shen et al., 2018; Zhao et al., 2019) in next work.

Data Availability

The DEMETER satellite data were provided by DEMETER scientific mission center (http://demeter.cnrs-orleans.fr). The GPS-TEC data were provided by CODE (Center for Orbit Determination in Europe) and can be downloaded from the website ftp://cddis.gsfc.nasa.gov/pub/gps/products/ionex. The COSMIC ,Dst and Kp index data can be obtained from the website https://cdaac-www.cosmic.ucar.edu/cdaac/cgi_bin/fileFormats.cgi?type=ionPrf; http://wdc.kugi.kyoto-u.ac.jp/dst_final/index.html; ftp://ftp.gfz-potsdam.de/pub/home/obs/kp-ap/wdc/yearly/ respectively.

Author Contributions:

Conceptualization, S.Z.; Formal analysis, S.Z.; Investigation, S.Z.; Methodology, S.Z., R.Z., and X.S.; Resources, S.Z., X.S. and R.Z.; Supervision, S.Z.; Visualization, S.Z.; Writing-original draft, S.Z.; Writing-review & editing, S.Z., R.Z, .C.Z., and X.S..

Corresponding author

Correspondence to Shufan Zhao.

Competing interests

The authors declare that they have no competing interests.

Funding:

This work is supported by the National Science Foundation of China (Grant No. 41704156, 41874174), National Key R&D Program of China (Grant No. 2018YFC1503501), the Special Fund of the Institute of Earthquake

369 Forecasting, China Earthquake Administration (Grant No: 2015IES010103, 2018CSES0203) and the APSCO

370 Earthquake Research Project Phase II.

371 **Acknowledgements**

372 This manuscript benefit from constructive review comments by two anonymous reviewers and editors. Thanks

373 for their advice and help. We acknowledge the DEMETER scientific mission center for providing data of

374 DEMETER satellite (http://demeter.cnrs-orleans.fr). The GPS-TEC data were provided by CODE (Center for

375 Orbit Determination in Europe) and can be downloaded from the website

376 ftp://cddis.gsfc.nasa.gov/pub/gps/products/ionex. The COSMIC ,Dst and Kp index data can be obtained from

377 the website https://cdaac-www.cosmic.ucar.edu/cdaac/cgi_bin/fileFormats.cgi?type=ionPrf;

378 http://wdc.kugi.kyoto-u.ac.jp/dst_final/index.html; ftp://ftp.gfz-potsdam.de/pub/home/obs/kp-ap/wdc/yearly/

379 respectively.

380

381 **References**

382 1. Bilitza, D., Altadill, D., Truhlik, V., Shubin, V., Galkin, I., Reinisch, B., and Huang, X.: International
383 Reference Ionosphere 2016: From ionospheric climate to real-time weather predictions. Space Weather-the
384 International Journal of Research & Applications 15, 418-429, 2017.

385 2. Budden, K., 1985. The Propagation Of Radio Waves: The Theory Of Radio Waves Of Low Power In The
386 Ionosphere And Magnetosphere. Cambridge University Press, Cambridge, United Kingdom.

387 3. Clilverd, M. A., Rodger, C. J., Gamble, R., Meredith, N. P., Parrot, M., Berthelier, J. J., and Thomson, N. R.:
388 Ground-based transmitter signals observed from space: Ducted or nonducted? Journal of Geophysical Research
389 Atmospheres 113, A04211, 2008.

390 4. Cohen, M. B., and Inan, U. S.: Terrestrial VLF transmitter injection into the magnetosphere. J. Geophys. Res.:
391 Space Phys 117, 2012.

392 5. Dobrovolsky, I. P., Zubkov, S. I., and Miachkin, V. I.: Estimation of the size of earthquake preparation zones.
393 Pure Appl. Geophys. 117, 1025-1044, 1979.

394 6. Finlay, C. C., Maus, S., Beggan, C. D., Bondar, T. N., Chambodut, A., Chernova, T. A., Chulliat, A.,
395 Golovkov, V. P., Hamilton, B., Hamoudi, M., Holme, R., Hulot, G., Kuang, W., Langlais, B., Lesur, V., Lowes, F.
396 J., Luhr, H., Macmillan, S., Mandea, M., McLean, S., Manoj, C., Menvielle, M., Michaelis, I., N., O., Rauberg, J.,
397 Rother, M., Sabaka, T. J., Tangborn, A., L., T.-C., Thebault, E., Thomson, A. W. P., Wardinski, I., Wei, Z., and
398 Zvereva, T. I.: International Geomagnetic Reference Field: the eleventh generation. Geophys J Int 183, 1216-1230,
399 2010.

400 7. Gousheva, M., Glavcheva, R., Danov, D., Angelov, P., Hristov, P., Kirov, B., and Georgieva, K.: Satellite
401 monitoring of anomalous effects in the ionosphere probably related to strong earthquakes. Advances in Space
402 Research 37, 660-665, 2006.

403 8. Gousheva, M., Glavcheva, R., Danov, D., Hristov, P., Kirov, B. B., and Georgieva, K.: Electric field and ion
404 density anomalies in the mid latitude ionosphere: Possible connection with earthquakes? Advances In Space
405 Research 42, 206-212, 2008.

406 9. Hayakawa, M.: VLF/LF Radio Sounding of Ionospheric Perturbations Associated with Earthquakes.
407 Sensors 7, 1141-1158, 2007.

408 10. He, Y., Yang, D., Chen, H., Qian, J., Zhu, R., and Parrot, M.: SNR changes of VLF radio signals detected
409 onboard the DEMETER satellite and their possible relationship to the Wenchuan earthquake. Science in China
410 Series D-Earth Sciences (in Chinese) 39, 403-412, 2009.

411 11. Inan, U. S., Golkowski, M., Casey, M. K., Moore, R. C., Peter, W. B., Kulkarni, P., Kossey, P., Kennedy, E.,
412 Meth, S., and Smit, P.: Subionospheric VLF observations of transmitter-induced precipitation of inner radiation
413 belt electrons. Geophys. Res. Lett. 34, L02106, 2007.

414 12. Inan, U. S., and Helliwell, R. A.: DE-1 observations of VLF transmitter signals and wave-particle
415 interactions in the magnetosphere. Geophys. Res. Lett. 9, 917–920, 1982.

13. Kong, J., Yao, Y., Zhou, C., Liu, Y., Zhai, C., Wang, Z., and Liu, L.: Tridimensional reconstruction of the Co-Seismic Ionospheric Disturbance around the time of 2015 Nepal earthquake. Journal of Geodesy 92, 1255-1266, 2018.

14. Kuo, C. L., Huba, J. D., Joyce, G., and Lee, L. C.: Ionosphere plasma bubbles and density variations induced by pre-earthquake rock currents and associated surface charges. J Geophys Res-Space 116, 2011.

15. Lehtinen, N. G., and Inan, U. S.: Radiation of ELF/VLF waves by harmonically varying currents into a stratified ionosphere with application to radiation by a modulated electrojet. J. Geophys. Res. 113, 2008.

16. Lehtinen, N. G., and Inan, U. S.: Full-wave modeling of transionospheric propagation of VLF waves. Geophys. Res. Lett. 36, 2009.

17. Li, Y., Zhang, L., Zhang, K., and Jin, X.: Research on the Atmospheric Electric Field Abnormality near the Ground Surface before"5. 12"Wenchuan Earthquake. Plateau and Mountain Meteorology Research 37, 49-53, 2017.

18. Liao, L., Zhao, S., and Zhang, X.: Advances in the study of transionospheric propagation of VLF waves. Chinese Journal of Space Science (in Chinese) 37, 277-283, 2017.

19. Liu, J. Y., Chen, Y. I., Chen, C. H., Liu, C. Y., Chen, C. Y., Nishihashi, M., Li, J. Z., Xia, Y. Q., Oyama, K. I., Hattori, K., and Lin, C. H.: Seismoionospheric GPS total electron content anomalies observed before the 12 May 2008 Mw7.9 Wenchuan earthquake. Journal of Geophysical Research: Space Physics 114, 2009.

20. Liu, J. Y., Chen, Y. I., Chuo, Y. J., and Tsai, H. F.: Variations of ionospheric total electron content during the Chi-Chi earthquake. Geophysical Research Letters 28, 1383-1386, 2001.

21. Liu, J. Y., Tsai, Y. B., Chen, S. W., Lee, C. P., Chen, Y. C., Yen, H. Y., Chang, W. Y., and Liu, C.: Giant ionospheric disturbances excited by the M9.3 Sumatra earthquake of 26 December 2004. Geophysical Research Letters 33, 2006.

22. Marshall, R. A., Inan, U. S., and Glukhov, V. S.: Elves and associated electron density changes due to cloud-to-ground and in-cloud lightning discharges. Journal of Geophysical Research: Space Physics 115, 2010.

23. Maurya, A. K., Venkatesham, K., Tiwari, P., Vijaykumar, K., Singh, R., Singh, A. K., and Ramesh, D. S.: The 25 April 2015 Nepal Earthquake: Investigation of precursor in VLF subionospheric signal. J Geophys Res-Space 121, 10403-10416, 2016.

24. Molchanov, O. A., Rozhnoi, A., Solovieva, M., Akentieva, O., Berthelier, J. J., Parrot, M., Lefeuvre, F., Biagi, P. F., Castellana, L., and Hayakawa, M.: Global diagnostics of the ionospheric perturbations related to the seismic activity using the VLF radio signals collected on the DEMETER satellite. Natural Hazards & Earth System Sciences 6, 745-753, 2006.

25. Namgaladze, A. A., Zolotov, O. V., and Prokhorov, B. E.: Numerical Simulation of the Variations in the Total Electron Content of the Ionosphere Observed before the Haiti Earthquake of January 12, 2010. Geomagn Aeronomy+ 53, 522-528, 2013.

26. Píša, D., Němec, F., Santolík, O., Parrot, M., and Rycroft, M.: Additional attenuation of natural VLF electromagnetic waves observed by the DEMETER spacecraft resulting from preseismic activity. Journal of Geophysical Research: Space Physics 118, 5286-5295, 2013.

27. Parrot, M., Benoist, D., Berthelier, J. J., Błęcki, J., Chapuis, Y., Colin, F., Elie, F., Fergeau, P., Lagoutte, D., and Lefeuvre, F.: The magnetic field experiment IMSC and its data processing onboard DEMETER: Scientific objectives, description and first results. Planetary & Space Science 54, 441-455, 2006.

28. Parrot, M., Sauvaud, J., Berthelier, J., and Lebreton, J.: First in-situ observations of strong ionospheric perturbations generated by a powerful VLF ground-based transmitter. Geophys. Res. Lett. 34, 2007.

29. Peter, W. B., Chevalier, M. W., and Inan, U. S.: Perturbations of midlatitude subionospheric VLF signals associated with lower ionospheric disturbances during major geomagnetic storms. J Geophys Res-Space 111, 2006.

30. Pokhotelov, D., Mitchell, C. N., Spencer, P. S. J., Hairston, M. R., and Heelis, R. A.: Ionospheric storm time dynamics as seen by GPS tomography and in situ spacecraft observations. J Geophys Res-Space 113, 2008.

31. Pulinets, S. A.: Physical mechanism of the vertical electric field generation over active tectonic faults. Advances In Space Research 44, 767-773, 2009.

32. Pulinets, S. A., Boyarchuk, K. A., Hegai, V. V., Kim, V. P., and Lomonosov, A. M.: Quasielectrostatic model of atmosphere-thermosphere-ionosphere coupling. Advances in Space Research 26, 1209-1218, 2000.

33. Shao, X., Eliasson, B., Sharma, A., Milikh, G., and Papadopoulos, K.: Attenuation of whistler waves through conversion to lower hybrid waves in the low-altitude ionosphere. J. Geophys. Res.: Space Phys 117, 2012.

34. Shen, X., Zhima, Z., Zhao, S., Qian, G., Ye, Q., and Ruzhin, Y.: VLF radio wave anomalies associated with the 2010 Ms 7.1 Yushu earthquake. Advances in Space Research 59, 2017.

471   35. Shen, X. H., Zhang, X. M., Yuan, S. G., Wang, L. W., Cao, J. B., Huang, J. P., Zhu, X. H., Piergiorgio, P., and
472   Dai, J. P.: The state-of-the-art of the China Seismo-Electromagnetic Satellite mission. Sci China Technol Sc 61,
473   634-642, 2018.

474   36. Stangl, G., Boudjada, M. Y., Biagi, P. F., Krauss, S., Maier, A., Schwingenschuh, K., Al-Haddad, E., Parrot,
475   M., and Voller, W.: Investigation of TEC and VLF space measurements associated to L'Aquila (Italy) earthquakes.
476   Nat Hazard Earth Sys 11, 1019-1024, 2011.

477   37. Starks, M. J., Quinn, R. A., Ginet, G. P., Albert, J. M., Sales, G. S., Reinisch, B. W., and Song, P.: Illumination
478   of the plasmasphere by terrestrial very low frequency transmitters: Model validation. J. Geophys. Res.: Space
479   Phys 113, 2008.

480   38. Tao, X., Bortnik, J., and Friedrich, M.: Variance of transionospheric VLF wave power absorption. J. Geophys.
481   Res.: Space Phys 115, 2010.

482   39. Xu, T., Hu, Y. L., Wu, J. A., Wu, Z. S., Li, C. B., Xu, Z. W., and Suo, Y. C.: Anomalous enhancement of electric
483   field derived from ionosonde data before the great Wenchuan earthquake. Advances In Space Research 47, 1001-
484   1005, 2011.

485   40. Yao, L., Chen, H., and He, Y.: The signal to noise ratio disturbance of ionospheric VLF radio signal before
486   the 2010 Yushu Ms7.1 earthquake. Acta Seismologica Sinica 35, 390-399, 2013.

487   41. Yeh, K. C., and Liu, C. H., 1972. Theory of Ionospheric Waves. Academic Press, New York.

488   42. Zhao, B. Q., Wang, M., Yu, T., Wan, W. X., Lei, J. H., Liu, L. B., and Ning, B. Q.: Is an unusual large
489   enhancement of ionospheric electron density linked with the 2008 great Wenchuan earthquake? J Geophys Res-
490   Space 113, 2008.

491   43. Zhao, S., Liao, L., and Zhang, X.: Trans-ionospheric VLF wave power absorption of terrestrial VLF signal.
492   Chinese Journal of Geophysics (in Chinese) 60, 3004-3014, 2017.

493   44. Zhao, S., Zhang, X., Zhao, Z., Shen, X., and Chen, Z.: Temporal variations of electromagnetic responses in
494   the ionosphere excited by the NWC communication station. Chinese Journal of Geophysics- Chinese Edition 58,
495   2263-2273, 2015.

496   45. Zhao, S., Zhou, C., Shen, X., and Zhima, Z.: Investigation of VLF transmitter signals in the ionosphere by
497   ZH-1 observations and full-wave simulation. Journal of Geophysical Research: Space Physics 124, 4697-4709,
498   2019.

499   46. Zhou, C., Liu, Y., Zhao, S. F., Liu, J., Zhang, X. M., Huang, J. P., Shen, X. H., Ni, B. B., and Zhao, Z. Y.: An
500   electric field penetration model for seismo-ionospheric research. Advances In Space Research 60, 2217-2232, 2017.

501   47. Zigman, V., Grubor, D., and Sulic, D.: D-region electron density evaluated from VLF amplitude time delay
502   during X-ray solar flares. J Atmos Sol-Terr Phy 69, 775-792, 2007.

503
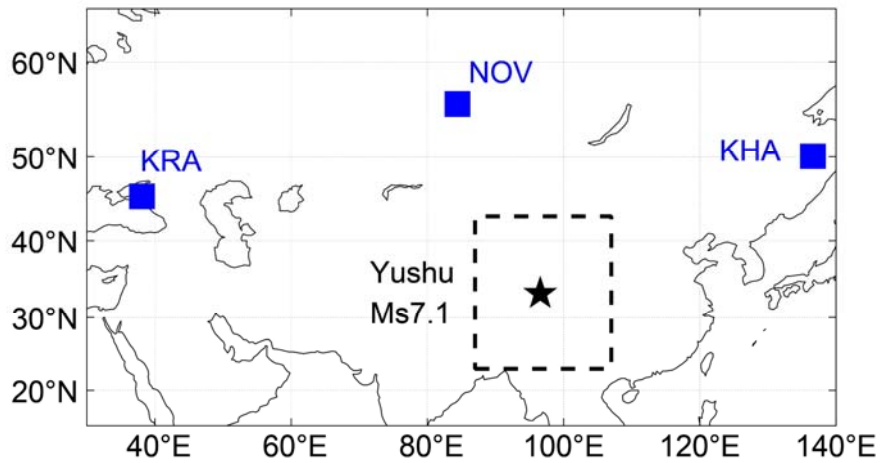
504

505 **Figure 1: The locations of transmitters and Yushu earthquake. The blue squares represent the**
506 **locations of the three transmitters (KRA, NOV, KHA) in Russia. The epicenter of Yushu earthquake**
507 **is denoted by the black star. The black square covers the region of epicenter ±10° in which the**
508 **data has been studied.**
509

510
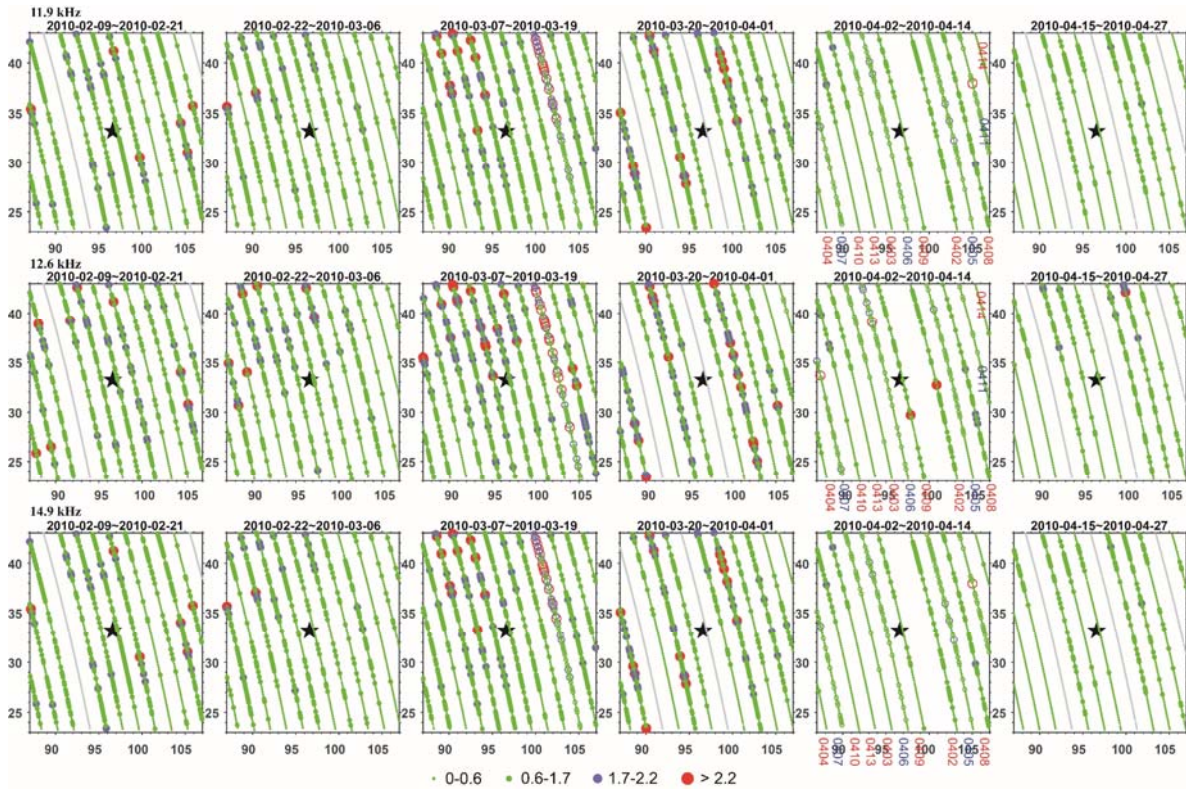
Figure 2: The evolution of SNR evolution VLF radio waves frequencies 11.9 kHz (top panel), 12.6 kHz (middle panel), 14.9 kHz (bottom panel) with Δf = 300 Hz at night time. The black star stands for the epicenter of the Yushu earthquake, the grey line represents the transmitter turns off on that day, the days with high geomagnetic activity are marked by blue color and hollow dots.

516
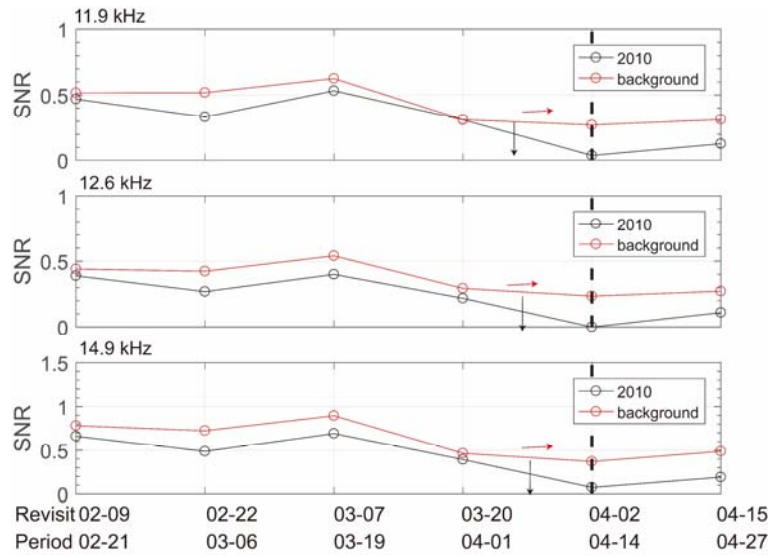
517 **Figure 3: The average SNR variation with revisit period inside the square region with the center of the**

518 **epicenter. The panel from top to the bottom are the SNRs at 11.9, 12.6, 14.9 kHz and the numbers of the**

519 **averaged data points. The green and red lines represent the SNR variations in 2010 and background time**

520 **separately. The black dashed line represents the period with the end date of main shock date.**

521

522
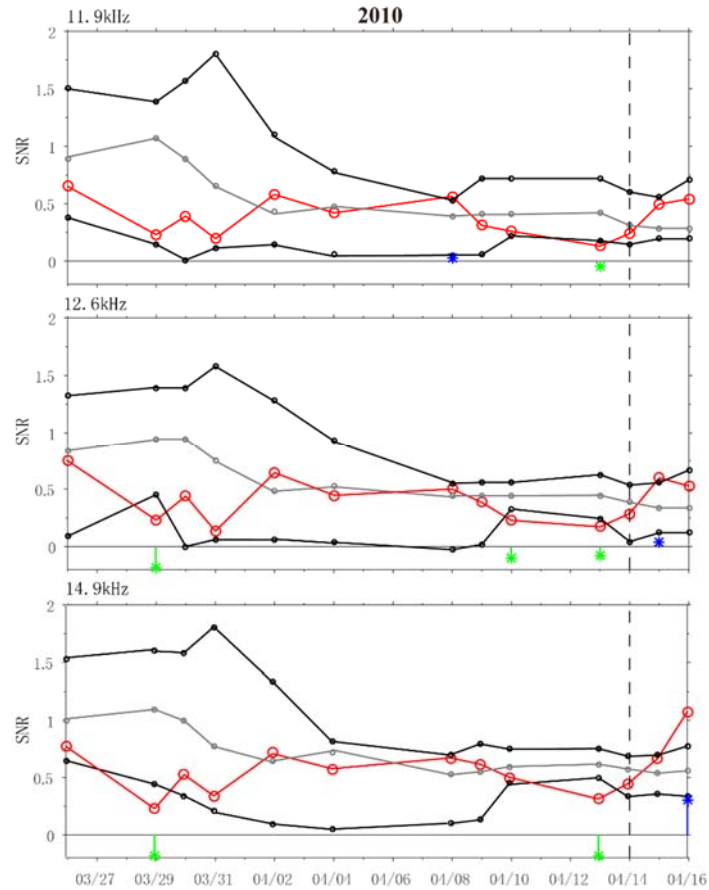
Figure 4: A time series of SNR right above the Yushu epicenter. The Ms 7.1 Yushu earthquake occurred at the local time 07:49:37.9 of April 14, 2010. The red, gray, and two black curves denote the current observed SNR and associated median and upper/lower bound (UB/LB), respectively. Blue and green sign represent the upper and lower anomalous days identified by the computer routine, respectively. The LB and UB are constructed by the 1–11 previous days' moving median (M), lower quartile (LQ), and upper quartile (UQ) and the LB and UB are calculated by LB = M+2(M-LQ) and UB= M+2(UQ-M) .
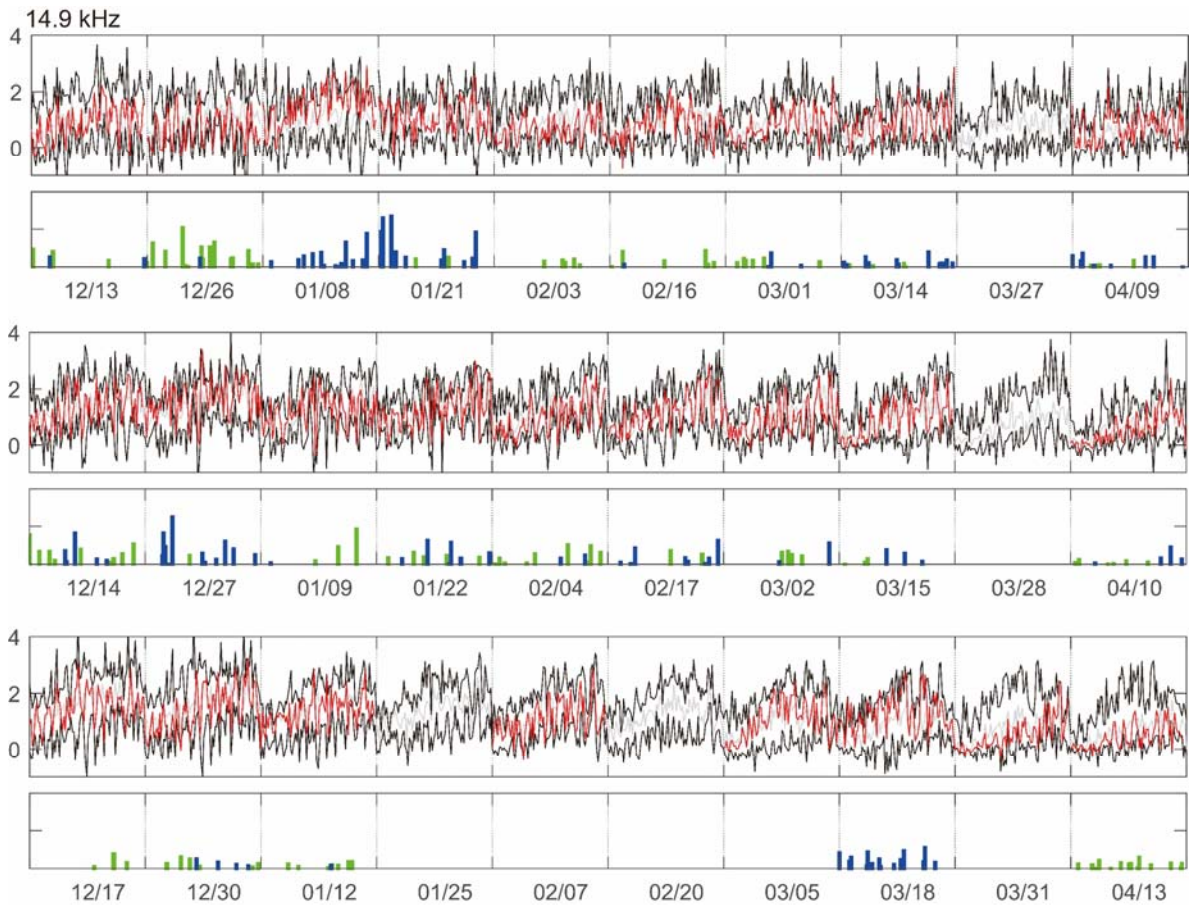
530
531 **Figure 5: A revisit orbital SNR of April 9,10,13,2010. The red, gray, and two black curves denote**
532 **the current observed SNR and associated median and upper/lower bound (UB/LB), respectively.**
533 **Blue and green bar represent the positive and negative anomalies in one orbit, respectively. The**
534 **LB and UB are constructed by the 6 days' moving median (M, including 3 days before current day,**
535 **2 days after current day), lower quartile (LQ), and upper quartile (UQ) and the LB and UB are**
536 **calculated by LB = M+2(M-LQ) and UB= M+2(UQ-M)**

537

538

Figure 6: The spatial distribution of GPS-TEC MAP (top) and its anomalies (bottom). The GPS-TEC

539

540 **MAP on April 13 at UT 6:00 (left of top panel). The sliding mean of 11 days of background (right of top**

541 **panel). The global anomalies in GPS-TEC MAP (left of bottom panel). The regional anomalies around**

542 **epicenter of Yushu earthquake in GPS-TEC MAP (right of bottom panel). The purple pentagram**

543 **indicates the epicenter and the radius of the black circle is 550km.**

544
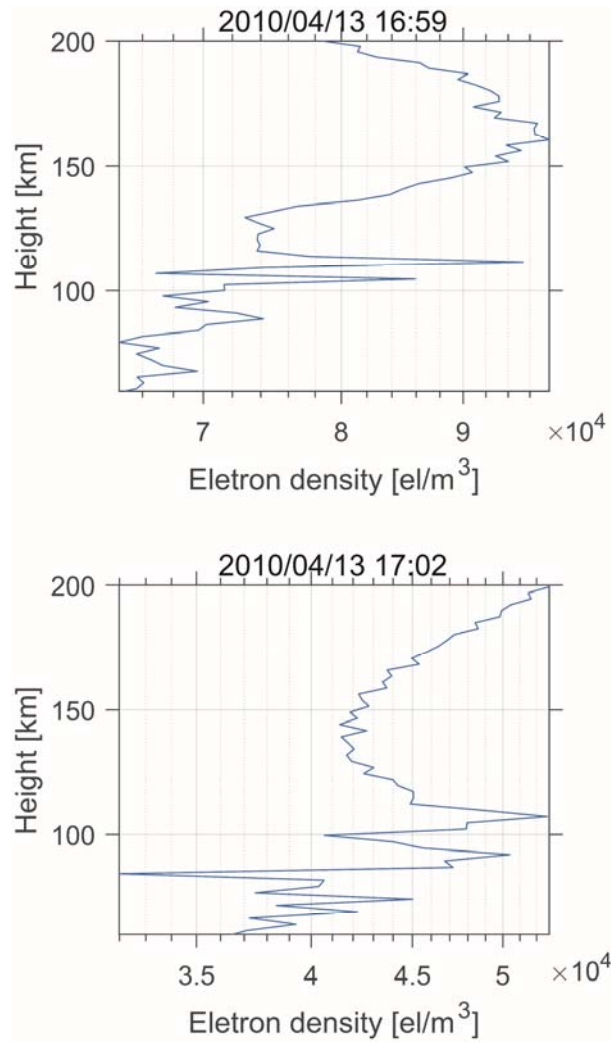
545

546 **Figure 7: The electron density obtained from COSMIC data on April 13 in the TEC abnormal region.**

547
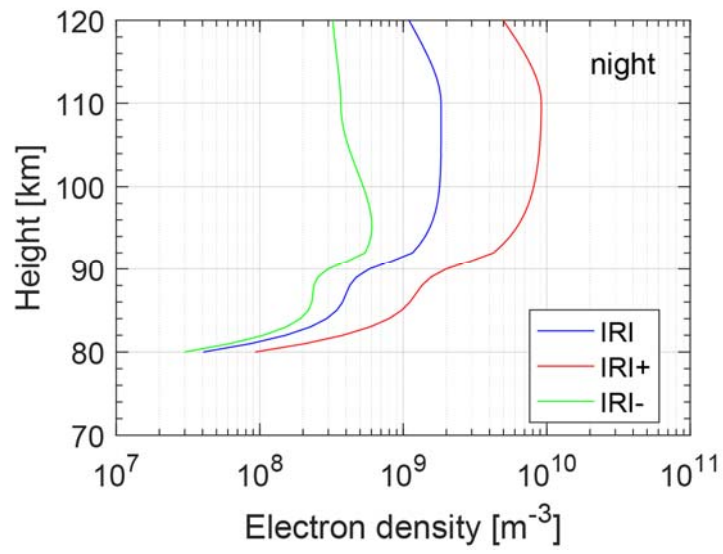
548

549 **Figure 8: The electron density profiles during night time. IRI represents the original electron density**
550 **predicted by IRI model; IRI+ represents the electron density added Gaussian shape perturbation; IRI-**
551 **represents the electron density subtracted Gaussian shape perturbation.**

552
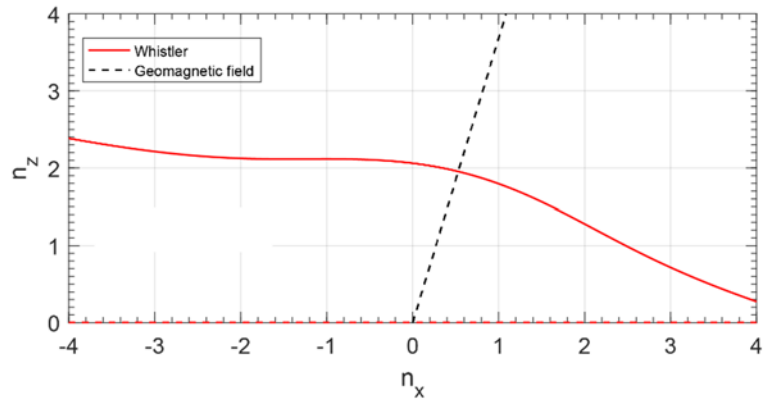
553

554 **Figure 9: The refractive index surface at 120 km. Red line shows a slice of the refractive index surface at**

555 $\mathbf{n_y = 0}$ **of the whistler mode, calculated for** $\mathbf{f = 11.9\ kHz}$ **at the altitude of** $\mathbf{h = 120\ km}$**. Black dash**

556 **line shows the direction of the geomagnetic field.**

557
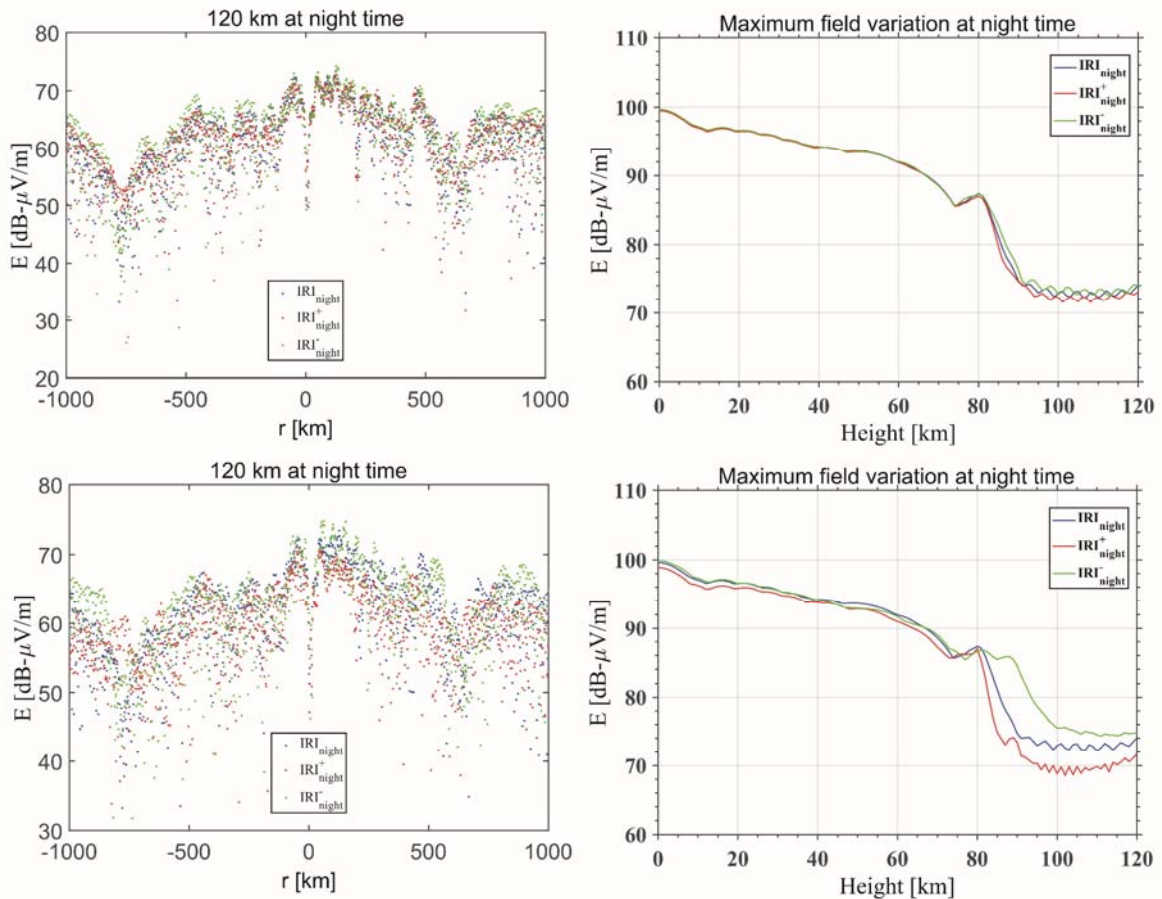
558
559 **Figure 10: The total electric field excited by ground based VLF transmitter NOV with transmitting**
560 **frequency f=11.9 kHz and power P=500 kW. The total electric field at the altitude of 120 km (a).**
561 **and the maximum electric field varying with altitude (b) in the nighttime when Gaussian shape**
562 **disturbance is set as 1.3 times compared with original electron density. The total electric field at**
563 **the altitude of 120 km (c). and the maximum electric field varying with altitude (d) in the**
564 **nighttime when Gaussian shape disturbance is set as 4 times compared with original electron**
565 **density.**
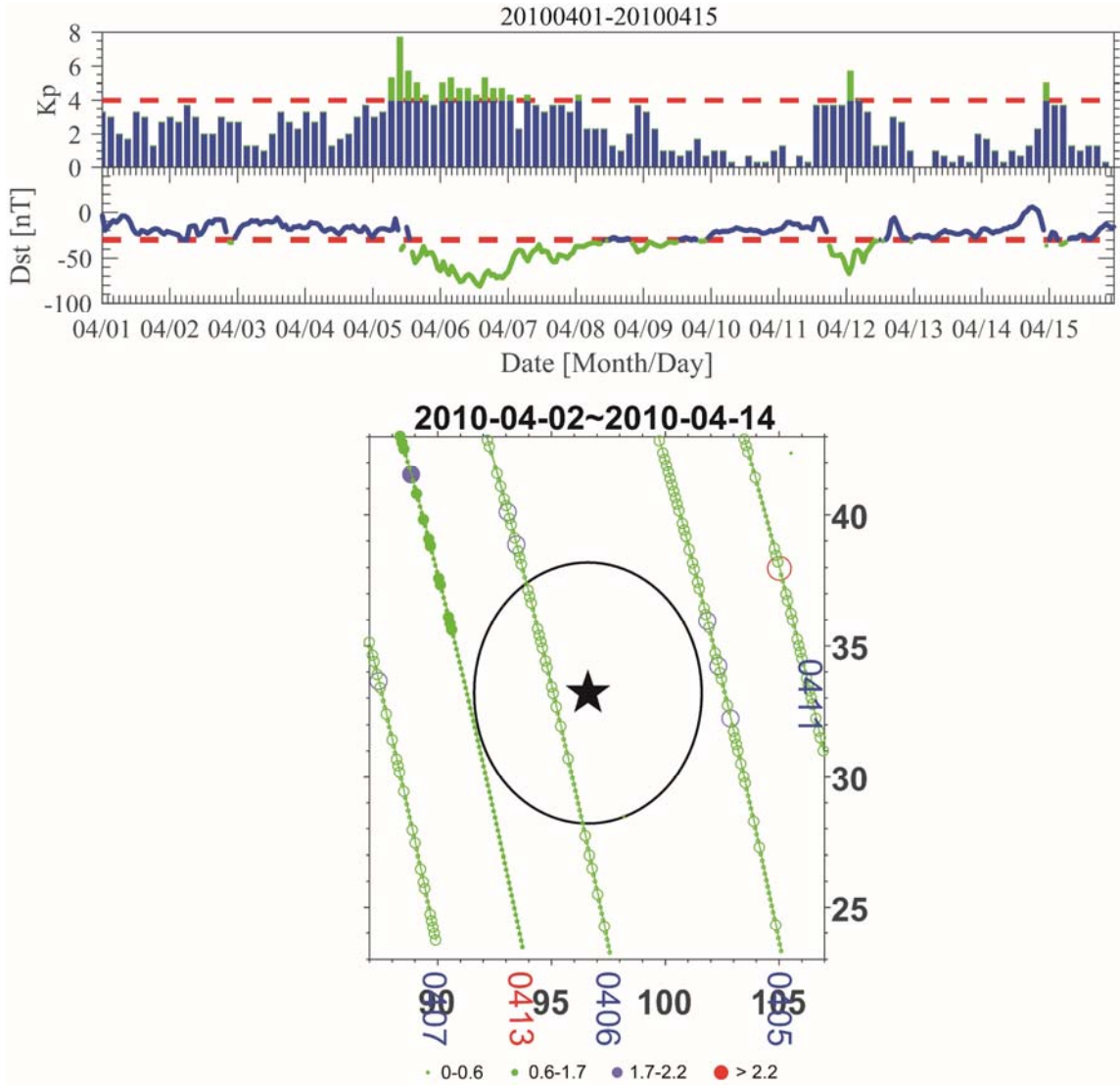
566

567 **Figure 11: The Kp and Dst index in April 2010 (top panel). The SNR distribution at April 5,6 with**

568 **geomagnetic storm and April 13 (one day before Yushu earthquake) (bottom panel).**